

Sustainable Ironmaking Toward a Future Circular Steel Economy: Exploiting a Critical Oxygen Concentration for Metallurgical Cu Removal from Scrap-Based Melts

Isnaldi R. Souza Filho,* Alisson K. da Silva, Ömer K. Büyüksulu, Dierk Raabe, and Hauke Springer*

A circular steel economy based on recycling scrap is severely hampered by the increasing accumulation of Cu returning from more and more electrified products, which severely limits processing, application, and safety of steels. As of yet, no viable strategies for its removal have been developed, and the increasing Cu contamination can only be diluted with fresh primary iron. This is not only evoking CO₂ emissions from conventional reduction processes, but also merely delays the problem until global demands allow for a circular steel economy. However, the ongoing transformation toward green steel making may offer pathways to overcome this complex metallurgical challenge. It is demonstrated that Cu can be effectively evaporated from Fe–Cu–O melts—representing Fe ore mixed with Cu-contaminated steel scrap—during hydrogen plasma-based smelting reduction. This evaporation is found to be strongly influenced by the Cu activity determined by the concentration of oxygen in the liquid, with a critical O concentration of about 22 wt%. Even without the presence of hydrogen, Cu concentrations can thereby be drastically reduced from 1 to less than 0.1 wt%. Potentials and challenges for leveraging these fundamental findings on a laboratory scale for future industrial production of green steel are outlined and discussed.

1. Introduction

Steel is not only the most important load-bearing metallic material,^[1] but it is also the most recycled material on the globe (e.g., ≈460 million tons of steel scraps were recycled in 2020).^[2,3] The recycled quantities already exceed those of all other materials combined, and fostering this trend represents a huge leverage to effectively and instantaneously fight global warming.^[4,5] The reason for this is that melting steel scrap in electric arc furnaces (EAFs) avoids the gargantuan CO₂ emissions from conventional blast furnace and oxygen converter production by up to 85%.^[6] This scenario is in reach and already realized in industry (i.e., crude steel production via a scrap-based EAF route), to a fraction of about 22% of the global market.^[7] However, an increasing use of mixed steel scrap means that impurity elements intrude and accumulate in the recycled steel.^[8–11] Most of these undesired additions can be removed during metallurgical


processing, for example by partitioning them into the slag.^[9] This does not, however, work for copper (Cu), an element that has two faces: it is a key enabler for sustainability,^[12,13] required for the electrification of production and transportation (Figure 1a),^[14] but it is also the most difficult element to remove from molten steel.^[15] Cu increasingly enters and contaminates scrap streams due to the growing amounts of electrical components (Figure 1b) and brazed joints in vehicles,^[14,16,17] thus developing into a grand challenge and serious obstacle in scrap-based green steel making.^[8] The difficulty to remove Cu from the molten scrap is due to its high solubility and thermodynamic stability in liquid Fe, which requires strategies based on low pressure atmospheres to induce its preferable evaporation, as its vapor pressure is higher than that of iron.^[18,19] Also, Cu is more noble than Fe, which impedes its conversion into more easily removable compounds such as slag-forming oxides.^[15]

The increasing amounts of Cu in steels start to cause serious and highly detrimental effects on steel manufacturing, application and product safety, with the so-called hot shortness—i.e., a dramatically reduced ductility at elevated temperature (>1000 °C)—as the most significant problem (an example of a

I. R. Souza Filho, A. K. da Silva, Ö. K. Büyüksulu, D. Raabe, H. Springer
Max-Planck-Institut für Eisenforschung GmbH
40237 Düsseldorf, Germany
E-mail: i.souza@mpie.de; h.springer@mpie.de

I. R. Souza Filho
Institut Jean Lamour
CNRS (UMR 7198)
Université de Lorraine
F-54000 Nancy, France

H. Springer
RWTH Aachen University
Metallic Composite Materials
52072 Aachen, Germany

 The ORCID identification number(s) for the author(s) of this article can be found under <https://doi.org/10.1002/srin.202300785>.

© 2024 The Authors. Steel Research International published by Wiley-VCH GmbH. This is an open access article under the terms of the Creative Commons Attribution-NonCommercial-NoDerivs License, which permits use and distribution in any medium, provided the original work is properly cited, the use is non-commercial and no modifications or adaptations are made.

DOI: 10.1002/srin.202300785

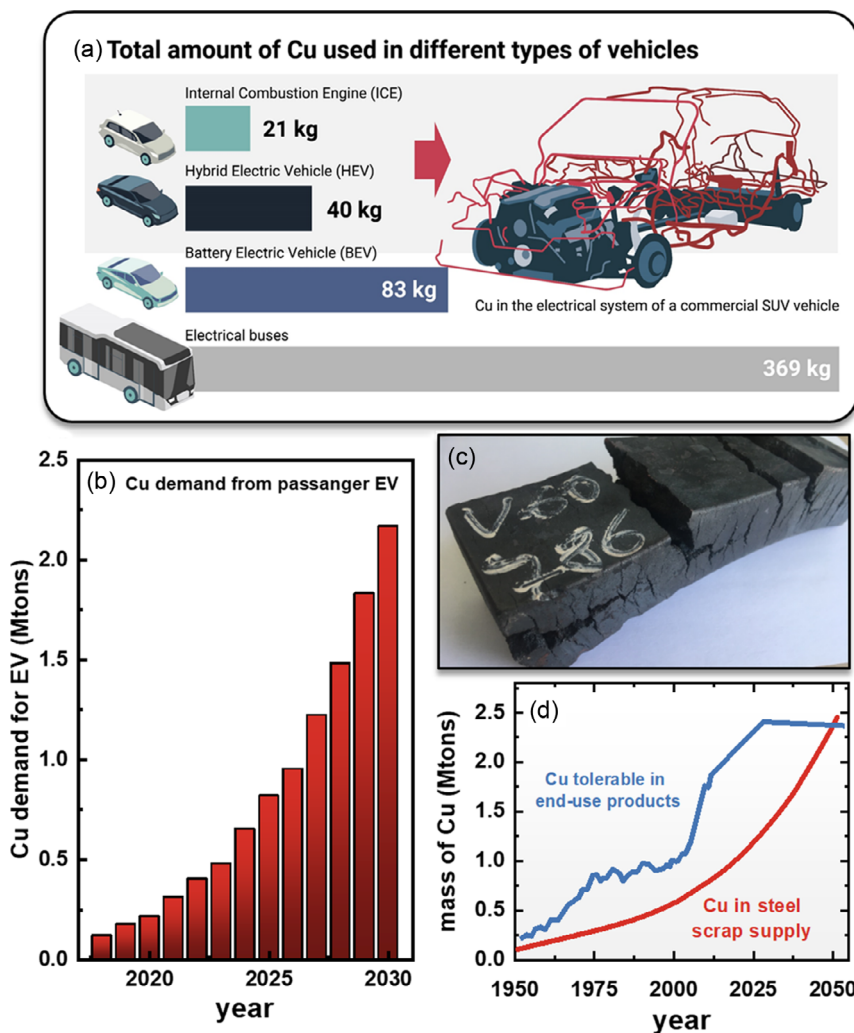


Figure 1. Current and future trends of the usage of Cu in electric vehicles. Structural problems caused by Cu contamination in steels; total amount of Cu utilized in electric vehicle (EV) variants (hybrid and battery electric ones) compared with the corresponding weight of 21 kg found in automobiles of internal combustion engine based on data from ref. [14]. Illustration of a Cu wire system in a commercial hybrid vehicle based on images from ref. [57]. b) Evolution and projection for 2030 of the Cu demands from electrical vehicles based on data from ref. [17]. c) Surface cracks induced by hot shortness in a Mn-containing steel sheet. d) Evolution of the quantities of Cu encountered in steel scraps versus the mass of Cu that is tolerable in end-use products. Reproduced under the terms of the CC-BY license.^[8] Copyright 2017, American Chemical Society, <https://doi.org/10.1021/acs.est.7b00997>.

steel plate compromised by hot shortness is shown in Figure 1c).^[20] It is caused by the formation of a liquid Cu-rich phase below the surface oxide scale during annealing of cast slabs, combined with the applied stresses of the hot forming processes such as forging or rolling. This severely limits the parameter window required for thermomechanical processing, the key step to transform mechanically inferior cast microstructures into high-performance structural materials. Together with other often unwanted effects such as precipitation hardening, the maximum limit of Cu in almost all commonly used steel grades is less than 0.1 wt%.^[9,11] However, the ever-growing accumulation of Cu in steel scraps is predicted to surpass by 2050 the concentration of Cu that is tolerable in end-use products, as shown in Figure 1d.^[8] This scenario will not only constrain the global steel recycling,

but also make the removal of Cu to remain as one of the key challenges for a circular steel economy.

However, a 100% circular steel economy is not yet possible, due to the still increasing global demand for steel.^[12] This means that feeding fresh Fe into the material flow chain remains necessary.^[21] This is the point where hydrogen comes into play, as an alternative reductant to the current fossil-based iron and steel making.^[22,23] We found that the use of hydrogen surprisingly opens up an excellent opportunity to solve both problems, i.e., the contaminant issue explained earlier, to enhance recyclability in steel making, and the decarburization of the primary sector, where Fe is currently produced from its ores through carbon-based reduction.^[24] Hydrogen-based reduction techniques are at the verge of widespread technical adoption, with solid-state

direct reduction^[23,25–27] already proven at industrial scale (e.g., through the Circored process^[28]) and the emerging hydrogen plasma reduction (HyPR)^[29–33] (pilot stage) as the most relevant processes. The latter is especially interesting from an energy efficiency standpoint,^[34] where Fe ore is molten and reduced in one step in a modified arc melting furnace under only small partial pressures of hydrogen (e.g., 10% H₂),^[29,30,35] ideally produced with renewable energy. While investigating the fundamental reduction reactions over HyPR, it was revealed that almost all accompanying elements brought in with the ore decrease in concentration, resulting in exceptionally pure Fe as the basis for steel production.^[29] Interestingly, also a reduction of the Cu content could be observed, albeit from rather small amounts (about 0.01 wt%) stemming from ore contamination.^[29]

The utilization of hydrogen-containing plasmas as a heating source to evaporate Cu from steels was already reported for smelting treatments at a low absolute pressure of 1.3×10^4 Pa.^[36,37] For the same purpose, other protocols also suggest the use of inert argon plasma treatments at even lower pressures (0.13×10^3 Pa).^[38] While the impact of the pressure on the Cu removal in molten steels—nearly devoid of oxygen—is clear, a thorough investigation about the role of the global oxygen content—specifically ranging from $\approx 30\%$ (Fe₂O₃) to 0% (Fe)—as a trigger for Cu evaporation in Fe-based melts has not yet been conducted. These observations motivated to investigate the potential to efficiently remove Cu from any iron or oxide melt, may it have intruded from the ores or from the scrap, in the context of HyPR, where O is constantly removed from the melt.

We found that Cu can be effectively evaporated from Fe–Cu–O melts when they reach a critical global oxygen content of ≈ 22 wt%. This fact motivated us to further investigate and confirm that the evaporation of Cu from mixtures of Cu-bearing steel scrap and fresh iron ore—whose global O content is near the critical one—also occur under inert argon plasma arcs. The Fe–O melt once purified from Cu (collected from the atmosphere of the reactor) can be processed with a reducing hydrogen plasma to achieve full conversion into metallic iron. Our approach combines primary synthesis and recycling; thus, it does rely on feeding fresh iron ore into the production chains. However, in this approach, the fresh feedstock is not simply aimed to dilute the undesired Cu (as the universally accepted solution for Cu contamination in steels), but rather it serves as an agent to effectively trigger its evaporation, thus offering also the potential to recover this valuable element for further use. With this work, we aim at providing scientific-based findings to help at least delay the projected time when a circular steel would be significantly hampered by the accumulated Cu amounts, as shown in Figure 1d.

2. Experimental Section

2.1. Synthesis of Fe–Cu and Fe–Cu–O Melts Containing 1 wt% Cu

To prepare the binary Fe–Cu and ternary Fe–Cu–O melts, 0.15 g of Cu flakes (99.98% purity) were respectively mixed with either 15 g of pure iron (99.99% purity) or 15 g of lab-grade hematite. The chemical composition of hematite was 28.9 wt% O, 0.10 wt% Si, 0.09 wt% Mn, 0.087 wt% Al, 0.025 wt% Ca, 0.048 wt% Mg,

0.04 wt% Ti, and traces of P, S, Na, K (with Fe as balance). The resulting composition of Cu in these mixtures was approximately 1% on a weight basis, i.e., the final composition of the binary and ternary mixtures was Fe–1%Cu and Fe–1% Cu–29%O, respectively.

2.2. Synthesis of Fe–Cu–O Melts Containing 22 wt% O

For the synthesis of the Fe–Cu–O melts containing a global oxygen composition of 22 wt%, ≈ 12 g of magnetite (97% purity on a metal basis) was mixed with 3 g of Fe scraps containing 1 and 5 wt% Cu. These mixtures are hereafter named “charge 1” and “charge 2”, respectively (e.g., in Figure 6). Magnetite was selected as the oxygen-carrier substance due to its lower tendency of undergoing thermal decomposition during heating and melting when compared with hematite (see Figure 4b), thus keeping the concentration of oxygen inside the melt as constant as possible around 22 wt% (see Figure 6b). However, when considering most abundant hematite ore variants, one might also evaluate the possibility of using an ore/scrap ratio of 2.75/1, thus also providing a global oxygen content of 22 wt%. This seemed to be of particular importance in the context of current HyPR pilot reactors which were mostly charged with hematite and required scraps as a facilitator agent for arc ignition (due to their higher electrical conductivity than that of FeO ores).^[39]

2.3. Processing of Fe–1%Cu and Fe–1%Cu–O Melts with Hydrogen Plasma

The processing of the mixtures synthesized according to the protocol described in Section 2.1 was performed in a small-scale Bühler arc melting furnace equipped with a tungsten electrode of 6.34 mm diameter. The Fe–Cu and Fe–Cu–O mixtures were independently placed on the water-cooled Cu hearth of the furnace, located immediately below the electrode. The furnace chamber (18 L) was flooded with a lean gas mixture of Ar–10%H₂ at a total pressure of 0.9×10^5 Pa. Simultaneous melting and reducing were achieved by igniting a plasma arc (length of ≈ 20 mm) between the tip of the electrode and the material at a current of 800 A. Complete melting was achieved with only 6 s of exposure to the plasma. Each sample was subjected to several melting/reducing-solidification cycles, varying from 1 to 15 ones. Each cycle lasted 1 min in total (i.e., during one single cycle, the sample was processed under plasma for 1 min). After the completion of each individual cycle, the furnace chamber was replenished with a fresh gas mixture of Ar–10%H₂ to provide adequate stoichiometric reducing atmospheres for the subsequent cycles. Rapid solidification conditions were imposed to the samples by the water-cooled Cu hearth once the arc was turned off.

2.4. Processing with Inert Argon Plasma

The magnetite/scrap samples prepared according to Section 2.2, and previously referred to as “Fe–Cu–O melts containing 22 wt% O”, were processed up to 30 min under argon plasma ignited at a lower current of 400 A, and not 800 A as in the case of the experiments described in Section 2.2. The same arc melting furnace

described in Section 2.3 was used to conduct the argon plasma-based processing experiments.

For the corresponding Fe–Cu–O melts with 1 wt% Cu and 29 wt% O, 15 g lab-grade hematite was mixed with 0.15 g of copper flakes (similarly to the procedure described in the Section 2.1). The mixtures were processed in the same arc melting furnace under an argon plasma ignited with a current of 800 A.

2.5. Microstructural and Chemical Characterization

After solidification, the representative Fe–Cu–O sample reduced for 5 min (with hydrogen plasma) was cut using a diamond wire. The corresponding cross section of this sample was metallographically prepared for high-resolution scanning electron microscopy (SEM) using a Zeiss Merlin microscope. To elucidate the local chemical partitioning of solidified sample, complementary energy-dispersive X-ray spectroscopy was employed at an accelerating voltage of 15 kV.

All solidified Fe–Cu and Fe–Cu–O samples were subjected to inductively coupled plasma optical emission spectrometry measurements for determination of the corresponding Fe and Cu contents. The oxygen content of the samples was inferred via phase stoichiometry, determined via Rietveld refinement of the X-ray diffraction (XRD) data acquired for the unreduced oxide portions of the Fe–Cu–O samples. For this purpose, these samples were hammered to magnetically separate their millimeter-sized iron domains from the oxide ones, as conducted in a preceding study.^[29] The latter portions were further crushed and the particles possessing sizes below 90 μm mesh was probed via XRD. XRD analysis were conducted using a D8 Advance A25-X1 diffractometer coupled with a cobalt $K\alpha$ X-ray source, and operated at 35 kV and 40 mA. Rietveld refinement was performed with the aid of the software Bruker Topas v. 5.0. Further details are given in a preceding work.^[29]

2.6. Thermodynamic Simulations

Equilibrium calculations were performed using the ThermoCalc software together with the TCS Metal Oxide Solutions Database (TCOX10) for the description of the liquid phases and the SSUB5 SGTE (Scientific Group Thermodata Europe) Substances Database for the description of the gas phase including metallic and oxide vapors. The liquid phase is described by a two sublattice model considering the following species: $(\text{Fe}^{2+}, \text{Cu}^+)_P(\text{VA}^{-Q}, \text{FeO}_{1.5}, \text{CuO}, \text{O}^{-2})_Q$, where charged vacancies and the stoichiometric factors P and Q which vary with the composition are introduced to keep electroneutrality.^[40–43]

3. Results

3.1. Plasma Smelting Experiments

Figure 2a shows a picture of a representative HyPR experiment conducted in an arc melting furnace filled with a gas mixture of Ar–10% H_2 (see Section 2.3). The arrow indicates the turbulent flow of the molten Fe ore caused by the direct interaction of the melt with the plasma arc. Such complex stirring events are

essentially indispensable for adequate mass transport toward the reaction interface between melt and plasma arc where the chemical reactions are effectively occurring over HyPR (Figure 2a), thus allow for the advancement of the process.^[44] Figure 2b displays the evolution of the Cu composition of a binary Fe–1%Cu alloy processed with both inert (Ar) and reducing (Ar–10% H_2) plasma. It shows that the concentration of Cu in this alloy slightly decreases to 0.6% only after 10 min exposure to the hydrogen containing plasma variant. Figure 2c depicts the changes in the O and Cu concentrations of a ternary Fe–O–Cu liquid mixture during argon plasma processing. This material was produced by mixing hematite (Fe_2O_3) plus 1% metallic Cu flakes, that is, its initial composition was ≈ 29 wt% O and 1 wt% Cu (Fe as balance). This figure shows that Cu remains nearly constant around 1 wt% over the process (horizontal line in Figure 1c). The O content decreases to 26 wt% after 1 min exposure to hydrogen-free Ar plasma, mainly due to thermal decomposition of the Fe oxide. Figure 2d depicts the chemical composition changes over HyPR of the same ternary Fe–O–Cu mixture composed of hematite plus 1% metallic Cu. In this case, the Cu concentration remarkably decreases from 1 to 0.1 wt% along with the reduction of the molten Fe oxide. This indicates that the presence of oxygen in the melt favors the Cu evaporation over the course of the hydrogen plasma reduction.

The O, Fe, and Cu losses that occur during reduction of the Fe–O–Cu-based melt are shown in Figure 2e–g, respectively. These figures illustrate that the Cu evaporation proceeds in three distinct regimes (vertical dashed lines). Figure 2g reveals that $\approx 75\%$ of the Cu that is dissolved in the molten material gets evaporated within the initial 5 min of process, occurring concomitantly with 50% reduction (i.e., 50% O loss, Figure 2e). Conversely, no appreciable Cu evaporation occurs within the process interval between 5 and 10 min, where full reduction is achieved. Most of the remaining Cu is removed by exposing the fully reduced material to a 10% hydrogen–argon plasma (15 min). These observations suggest that the Cu evaporation is dependent on the O global concentration of the Fe–O–Cu melt. The content of Fe maintains nearly unchanged during 1 min reduction and only $\approx 8\%$ of Fe loss occurs with 5 min of exposure to hydrogen plasma (Figure 2f). In the final stages of the reduction process, i.e., between 5 and 10 min, we observe an undesired evaporation of Fe (up to 20%) while no substantial evaporation of Cu occurs. This observation suggests that there is an optimal reduction interval where Cu can be removed from the Fe–Cu–O without losing valuable Fe.

Figure 3a shows the solidified Fe_2O_3 –1%Cu mixture after 5 min reduction. The remaining iron oxide domains are found atop a millimeter-sized iron portion (shiny contrast) which is located in the bottom of the sample. The region highlighted as “1” in Figure 3a was further probed via high-resolution SEM. The microstructure of the oxide portion and the corresponding local chemical partitioning are shown in Figure 3b. This figure shows a few micron-sized Fe domains entrapped within wüstite (Fe_xO) dendrites due to the fast solidification rates imposed by the adopted experimental conditions (Section 2.1). Copper is preferentially partitioned to such Fe domains. Figure 3c shows a detailed inspection of the interdendritic regions of the microstructure, particularly the one labeled as “2” in Figure 3b. Figure 3c shows a metallic submicron-sized

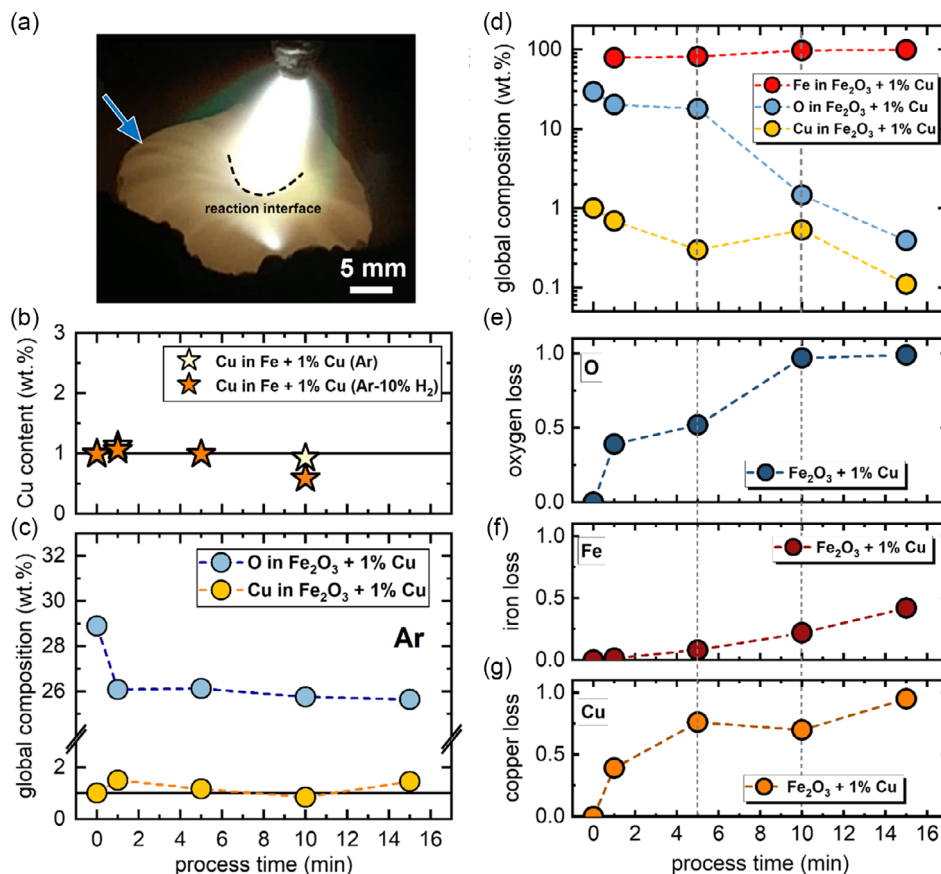


Figure 2. Experimentally determined chemistry of the Fe–Cu binary and Fe–Cu–O ternary systems exposed to both inert argon and reducing hydrogen-containing plasmas. a) Picture of the HyPR process. The arrow indicates the turbulent flow of the melt. b) Changes in Cu content of a binary Fe–1%Cu alloy processed under both inert Ar and reducing Ar–10% H_2 plasmas. c) Changes in O and Cu contents in a Fe–O–Cu liquid system originally containing ≈ 29 wt% O and 1 wt% Cu (Fe as balance) after melting with Ar plasma. d) Changes in the global chemical composition of a Fe–29%O–1%Cu system over exposure to a lean hydrogen plasma (Ar–10% H_2). Corresponding individual element losses in terms of e) O, f) Fe, and g) Cu. Cu evaporation occurs in three distinct regimes during HyPR as indicated by the vertical dashed lines. The arc plasma was ignited at a current of 800 A in all experiments.

Cu particle, suggesting strong local deviations from the equilibrium where all Cu is expected to be dissolved either in the iron or oxide phases.

3.2. Thermodynamic Simulations

The reduction of the Cu-containing molten Fe oxide under equilibrium conditions was calculated with the aid of thermodynamic simulations using the software Thermo-Calc in conjunction with the databases TCOX10 and SSUB5 SGTE (see Section 2.4). For this purpose, it was set as an initial condition a 10 g oxide liquid with a chemical composition of 29 wt% O and 1 wt% Cu (Fe as balance), i.e., the composition pertaining to the mixture of Fe_2O_3 plus metallic Cu that was investigated here. The molten material was kept at a constant temperature of 1850 °C and increasing quantities of a gas mixture of Ar–10% H_2 were added to the system. This means that the system is not a closed one and elemental partitioning is permitted between the liquid and gas phases during the simulations. The total pressure was 0.9×10^5 Pa. The temperature of 1850 °C was chosen based on the minimal

interfacial temperature of a hydrogen plasma arc and liquid iron, as estimated in ref.[37].

Figure 4a shows the changes in the absolute mass (in grams) of the different constituents, namely, gas and oxide and metallic liquids as a function of the amount of hydrogen added to the system (given in grams). Correspondingly, Figure 4b shows the evolution of the global oxygen of the molten material (grey curve) together with the reduction degree (golden curve), which was calculated based on the oxygen loss from the oxide liquid. In this figure, the horizontal dashed line indicates an oxygen loss of about 13% (viz., reduction), induced by the thermal decomposition of Fe_2O_3 when submitted to the boundary conditions adopted in the calculations.

Under equilibrium conditions, metallic liquid starts forming at a reduction degree of 34% which is achieved by exposing the oxide liquid to about 0.3 g of hydrogen (Figure 4a,b). At this reaction stage, the global O content of the melt is 22.3 wt% (Figure 4b). Further reaction promotes the gradual formation of the Fe-enriched liquid so that the full conversion is achieved with ≈ 0.9 g of hydrogen. The two vertical dashed lines in

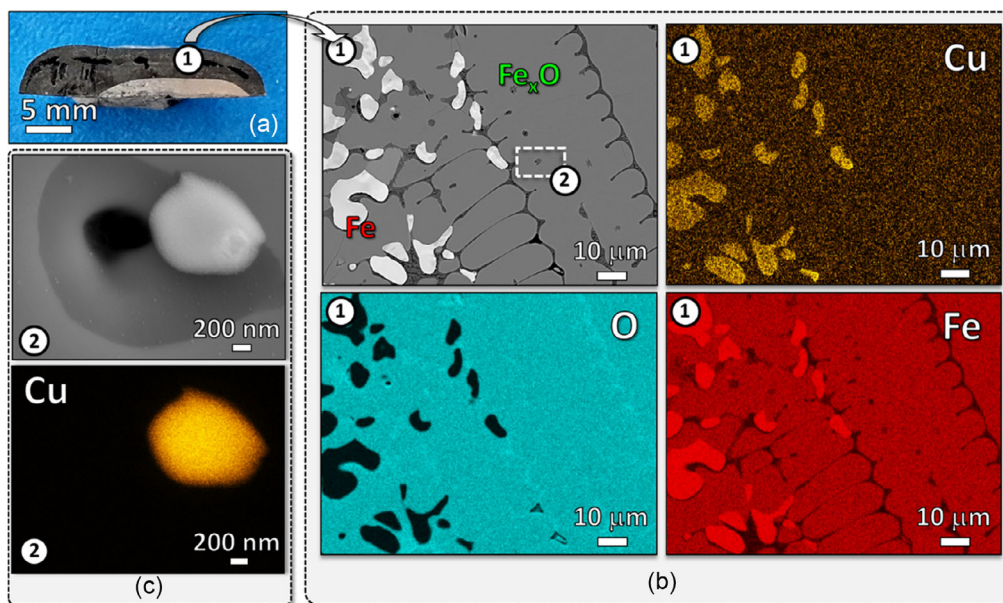


Figure 3. Microstructural and local chemical characterization of the Fe–Cu–O melt partially reduced with hydrogen plasma. a) Cu-containing Fe_2O_3 sample reduced for 5 min under a lean hydrogen plasma Ar–10% H_2 . b) Microstructure of the specimen visualized in the region labeled as “1” in (a). The corresponding local chemical partitioning is also given in terms of elemental maps for Fe, O, and Cu; c) detail of the interdentritic region of the sample (labeled as “2” in (b)), revealing the presence of a copper particle with a size of $\approx 1 \mu\text{m}$.

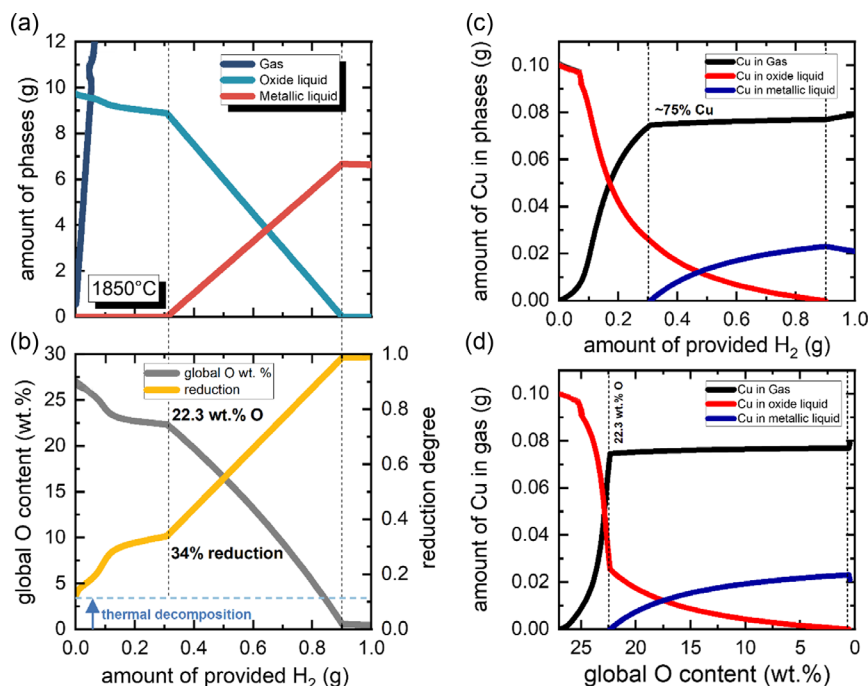


Figure 4. Thermodynamic simulations of the hydrogen-based reduction of a Fe–Cu–O melt at 1850 °C. a) Evolution of the absolute mass of the constituents of the system as a function of the provided hydrogen (in the form of a gas mixture of Ar–10% H_2). The vertical dashed lines highlight the miscibility gap between the oxide and metallic liquids. b) Evolution of the global oxygen content of the Fe–Cu–O melt exposed to deliberative increasing amounts of hydrogen (grey curve). Corresponding reduction degree calculated based on the oxygen loss of the oxide liquid (golden curve). Evolution of the Cu content (in grams) in all constituents of the system as a function of c) provided amounts of hydrogen and d) as a function of the global oxygen content of the system.

Figure 4a,b highlights the miscibility gaps between oxide and metallic liquids.

Figure 4c shows the Cu partitioning among the gaseous and liquid constituents as a function of the increasing quantities of H₂ molecules (provided to the system as a gas mixture of Ar–10% H₂) inserted into the system. Cu preferably evaporates from the oxide liquid in the early stages of reduction so that ≈75% of all Cu contained in the melt is partitioned into the gas before the formation of metallic liquid. For the reduction interval progressing along the miscibility gap (i.e., the interval delimited by the vertical dashed lines in Figure 4c), there is an apparent stagnation of Cu evaporation. This means that the remaining Cu dissolved in the oxide liquid partitions preferably to the metallic melt rather than evaporating. Further evaporation of Cu only occurs by over-exposing the fully converted metallic liquid to quantities above 0.9 g H₂ (Figure 4c). Figure 4d reproduces the findings observed in Figure 4c as a function of the global oxygen of the melt. This figure clarifies that the substantial evaporation of Cu (≈75%) occurs for O concentrations of up to 22.3 wt%.

While the results conducted for a temperature of 1850 °C display a fair agreement with the experimental Cu evaporation trends documented in Figure 2g, temperature gradients can certainly exist from the melt zones directly underneath the cathode toward the side walls of the furnace, that is, we can assume temperatures between 1850 and 2000 °C at the reaction interface,^[37] whereas the regions far from the electrodes might be slightly above the melting point of the Fe and FeO oxides (e.g., 1650–1700 °C). In fact, typical tapping temperatures commonly found in industrial arc melting furnaces are close to of 1650 °C.^[45] To investigate the impact of the temperature on the preferential evaporation of Cu, and eventual undesired evaporation of Fe from Fe–Cu–O melts, the thermodynamic calculations displayed in Figure 4 were reproduced for a temperature range between 1650 and 2000 °C, as shown in **Figure 5**.

Figure 5a,b show the fractions of Cu and Fe, respectively, partitioned to the gas phase over the course of hydrogen-based reduction of a Fe–29%O–1%Cu melt. For the sake of clarity, the calculated values are plotted against the global oxygen content ranging from 27% to 20%. These figures reveal that up to ≈50%

of the total Cu can be removed from the melt at typical tapping temperatures (1650–1700 °C) while maintaining the losses associated with Fe at a negligible level (≈0.3%). At 1850 °C, and as experimentally observed in Figure 2f,g, a substantial Cu evaporation of ≈75% is accompanied of a minor Fe loss of only 2%. At higher temperatures, i.e., at regions immediately underneath the plasma arc, the evaporation of Cu can be as high as ≈90%; however, one should consider that the accompanying evaporation of Fe can increase up to 8%. In all cases, the maximum evaporation of Cu is reached at about 22 wt% O, immediately preceding the formation of metallic Fe.

These results were obtained under equilibrium conditions and do not consider the highly reactive hydrogen species existing in a reducing plasma (e.g., H, H⁺, H^{*})^[33,46] and the kinetics-associated aspects of the experimental process (i.e., mass transportation to the hotter zones existing at the reaction interface, i.e., melt/plasma interface).^[47] However, they present a fair agreement with the findings obtained experimentally, suggesting that Cu evaporation over the course of the hydrogen-based reduction of molten iron ores is thermodynamically feasible.

4. Discussion

The results in Figure 2 suggest that Cu removal is highly dependent on the global O concentration of the molten material. The simulation results in Figure 4 and 5 also evidence the thermodynamic feasibility of Cu removal from Fe–Cu–O melts, underpinning the experimental observations (Figure 2). To better understand the corresponding underlying mechanisms, thermodynamic calculations were conducted and the results are shown in **Figure 6**. This figure shows the distribution map for the activity values of Cu in the Fe–Cu–O ternary liquid system. These values are plotted as a function of the global O and Cu contents at a fixed temperature of 2000 °C (this temperature was chosen here to exemplify as close as possible the scenario existing at regions of the melt existing immediately underneath the cathode, i.e., at the reaction interface). The map in Figure 6 reveals that the Cu activity reaches a maximum value at a global O

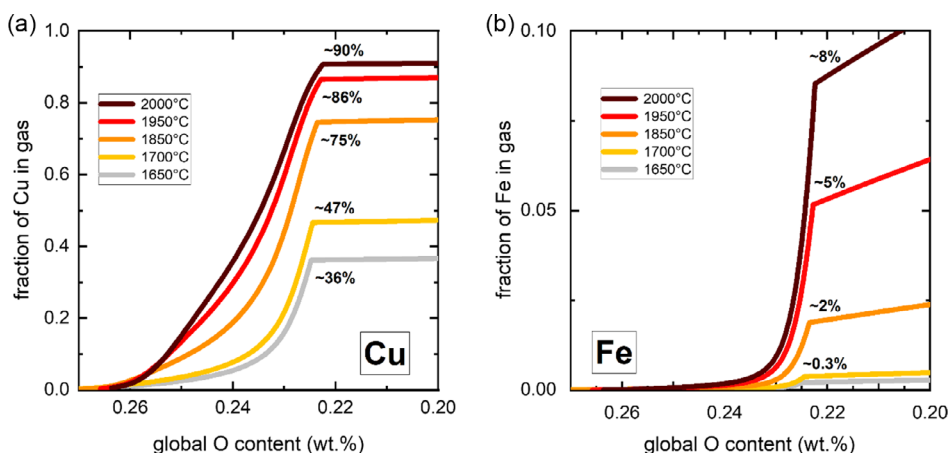


Figure 5. Thermodynamic simulations of the hydrogen-based reduction of a Fe–Cu–O melt at temperatures ranging from 1650 to 2000 °C. a) Fraction of the total Cu partitioned into the gas phase. b) Corresponding fractions of the total gas that evaporates by exposing the melt to increasing amounts of a gas mixture of Ar–10H₂. Results are plotted as a function of the global oxygen content of the liquid system.

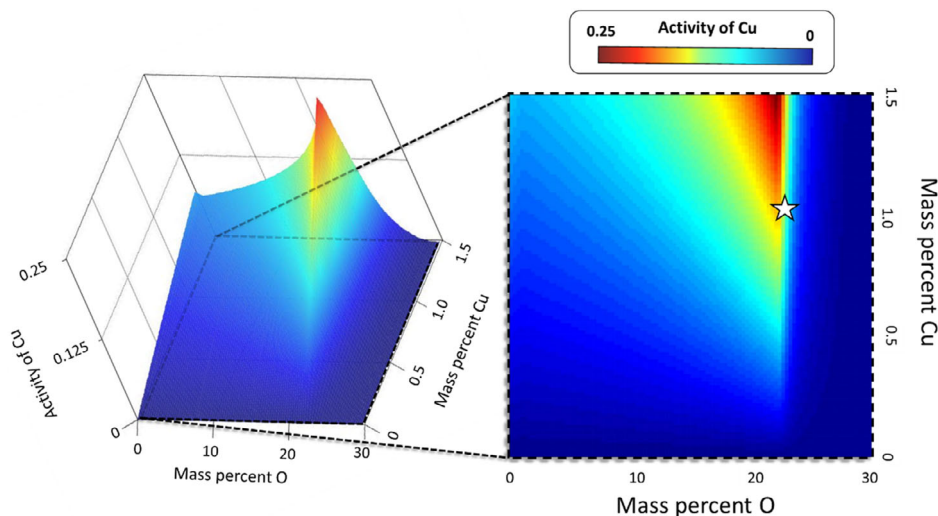


Figure 6. Distribution map for the Cu activity in a Fe–O–Cu ternary system. The corresponding values are plotted as function of global oxygen and copper composition (in wt%) at a fixed temperature of 2000 °C. The metallic liquid at 2000 °C was selected as the reference state for the metallic components and gaseous oxygen as the reference state for oxygen. The star symbol highlights the maximum Cu activity at a global O content of 22 wt% for a representative Cu concentration of 1 wt%.

composition near 22 wt% (marked by the star-shaped symbol for a representative global Cu composition of 1 wt%). At this O concentration, the maximum copper evaporation rate was inferred from the simulations shown in Figure 4d and 5b as well. These observations suggest that the Cu activity in the liquid solution, which is strongly affected by the O content, determines its evaporation, in accordance with the Raoult’s law,^[48] modified for nonideal mixture cases, i.e., the vapor pressure of an element in the vapor phase is directly proportional to its activity in the corresponding liquid solution.

The activity a is a convenient representation of the “effective concentration” of a given component in a mixture and it is related to the chemical potential μ_i of the component i through the relation:^[49]

$$a_i = e^{\frac{\mu_i - \mu_i^\theta}{RT}} \quad (1)$$

where μ_i^θ is the reference chemical potential of the component i , R is the gas constant, and T is the absolute temperature. Since the chemical potential is given by the partial molar derivative of the Gibbs energy in function of the amount of this component, the increase of the Cu activity with the decrease of the O content in the oxide liquid relates directly to the higher affinity of O with Fe as compared to Cu. The “effective concentration” of Cu in the liquid increases with the decrease of the O content (i.e., within the interval from 30 to ≈ 22 wt% global oxygen) because the change of Gibbs energy related to the formation of Fe–O-based substructures (e.g., $\text{FeO}_{1.5}$) in the liquid is lower than that one related to the formation of Cu–O-based ones (e.g., Cu_2O) in the same liquid. Therefore, copper is less effectively bonded inside the ionic liquid and evaporates more easily in the form of metallic Cu vapor, as O is removed. With further removal of oxygen and beyond a global O composition of 22 wt%, the formation of metallic liquid proceeds and the interaction between

Cu and Fe becomes predominant. Thus, the activity of Cu is reduced and its evaporation gets more difficult.

The current industrial solution to keep the Cu concentrations within steels below critical levels relies on diluting with fresh primary iron. This only delays the problem for future generations though (Figure 1d), as sooner or later, once global demand induced by infrastructure development is met, only losses by for example corrosion and wear would need replenishing. Such a future circular steel economy, while being extremely attractive due to the substantial energy savings it allows for, would be significantly hampered by the Cu concentrations accumulated to this point. Furthermore, a considerable amount of valuable Cu would become trapped within the global steel value chain and thereby become unavailable for other products being critically dependent on it, particularly in sectors highly associated with electrification (e.g., the electrified transport sector).

It thus becomes clear that it is of enormous importance to actively utilize the remaining time when the production of fresh primary iron based on the reduction of ores is still required and done on a large global scale. Interestingly, the findings documented in Figure 6 indeed suggest that new opportunities exist in the framework of an already transforming steel industry. However, not via the already established secondary production route of remelting scraps in EAF-based “mini mills”, but rather to switch streams and use the Cu contaminated steel scrap in the primary steel production route. As sketched in Figure 7a, the observed peak of Cu activity in the Fe–Cu–O liquid system can be exploited to remove Cu from the molten constituents for clean iron production. The hypothesis is that Fe scraps which are contaminated with Cu, could be molten in an arc melter (ensuring reliable ignition), and then subsequently add Fe ore so that the resulting mixture displays a chemical composition in terms of O near the critical one (represented in Figure 7a as a “critical O interval” to consider possible experimental

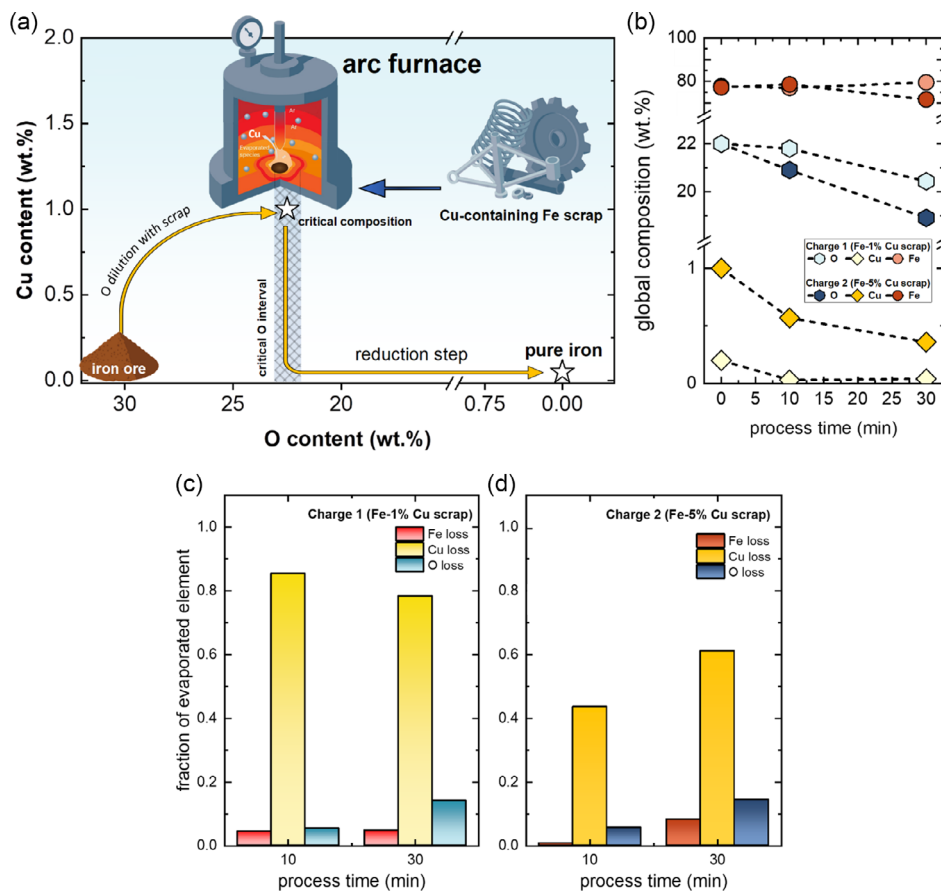


Figure 7. Theoretical scenario to remove Cu from steel scraps during primary iron production in future HyPR reactors or even in modified EAFs. a) Schematic representation of the plasma-based Cu evaporation route proposed in this work. b) Changes in Fe, Cu, and O contents of a feedstock composed of Fe ores (magnetite) and a Cu-containing Fe scraps (Fe-1%Cu and Fe-5%Cu, respectively, referred to as charges 1 and 2), both simultaneously charged into the same reactor and processed under inert argon plasma. Fraction of elements evaporated over the experiments with c) charge 1 and d) charge 2.

deviations). At this condition, melting the material with an inert plasma arc (e.g., argon) would enable enhanced evaporation of Cu without the need for using a reducing hydrogen-containing plasma (Figure 7a). Once the Cu amount is considerably reduced to acceptable levels, the inert plasma can be replaced by the moderately reducing one, to transform the oxide liquid into pure iron (see “reduction step” in Figure 7a), at optimal (low) fractions levels of the costly green hydrogen.^[30,50,51] The reduction step, however, could also be conducted with another reducing agent as C-based substances (in the case of conventional ironmaking routes) or greener ones (e.g., ammonia).

The validation of this hypothesis was performed with a new set of experiments in which a 15 g liquid Fe–Cu–O system was fabricated by mixing magnetite and Cu-containing Fe scraps (namely, Fe-1%Cu and Fe-5%Cu scraps and respectively named as “charge 1” and “charge 2” in Figure 7b), see Section 2.2. These hypothetical scraps, containing Cu amounts beyond those values observed in scraps processed through shredders and other conventional scrap sorting approaches (0.2–0.4 wt%),^[52] were used here to showcase the potential of the proposed approach in extreme cases of contamination. The global O composition of

the resulting mixtures was ≈ 22 wt%, which nearly coincides with the critical one. The global Cu content in the charges 1 and 2 are 0.2 and 1 wt%, respectively. The materials were processed for 10 and 30 min under an inert argon plasma ignited at 400 A under an absolute pressure of 0.9×10^5 Pa. With 30 min of process, the concentration of oxygen in the melt slightly decrease to 21% (charge 1) and 19% (charge 2)—Figure 7b, most likely due to thermal evaporation. The evaporation of Cu was remarkably achieved in both melting experiments, as revealed in Figure 7b–d) that shows the fraction of elements partitioned into the gas during the melting of charges 1 and 2, respectively. Figure 7c shows that the absolute Cu loss reaches $\approx 85\%$ for the charge 1 with a small competing Fe evaporation of only 4%, thus agreeing with the thermodynamic calculations reported in Figure 4 for the temperature of 1950 °C. Figure 7d also shows that appreciable $\approx 60\%$ of all Cu in charge 2 (which is five times more enriched in Cu than charge 1) was evaporated after 30 min melting, thus validating the concept of the proposed method even in scenarios of extreme high contamination.

To shed light on the thermodynamic possibility of applying our method in a modified EAF, containing refractory lining

chemically resistant against aggressive acidic FeO-based melts^[53] and operated under oxidizing atmospheres (i.e., air), we performed a new set of calculations where 10 g of a Fe–O–Cu melt displaying 22 wt% O and 1 wt% Cu (Fe as balance) was exposed to deliberative increasing amounts of air (i.e., 79% N₂ and 21% O₂) at temperatures ranging from 1650 to 2000 °C and under atmospheric pressure. The maximum amount of oxygen provided was 100 g (which corresponds to a total of ≈15 moles of air), representing ≈20 melting cycles in our lab-scale furnace (Section 2.1) or approximately 20 min of processing. The obtained results are shown in **Figure 8**. This figure reveals that, from a thermodynamic perspective, Cu can also be evaporated at the critical oxygen composition even under an oxidizing atmosphere. This analysis also reveals that the magnitude of the Cu evaporation is dependent on the temperature of the system, with ≈80% evaporation in regions possibly existing near the reaction interface (at 2000 °C, Figure 8a) and ≈20% occurring in positions far from the electrodes (1650 °C, Figure 8b). The losses associated with the absolute masses of Fe can reach a maximum of 1% at 2000 °C, but it is as negligible as 0.02% at 1650 °C. These findings might open the path for using Cu-containing scraps in pilot and future industrial HyPR reactors that require scraps on top of the charged ore to facilitate the initial ignition of the arc. In this sense, one might also consider the possibility of evaporating Cu under air while melting the whole volume charged into the reactor, allowing for liquefying the system without costly hydrogen or other inert gases. Thus, melting and purification of the melt together with recovery of Cu from the off-gas could occur in the preceding stages of the hydrogen-plasma reduction of the Fe–O melt.

Our experimental process model is scaled for a small volume, therefore, representing only the core of the plasma-based processes (e.g., HyPR), i.e., the liquid zone directly underneath the plasma.

Although process time and kinetics are not directly transferable to an industrial scale production, the model can be applied for studying fundamental metallurgical chemistry of the HyPR, Ar plasma, and EAF melting routes. The approach as sketched in Figure 7a does of course still rely on feeding fresh ore into the chain of production. However, it is now—in this approach—not

simply used for diluting the undesired Cu, but rather to effectively remove it, thus offering also the potential to extract this valuable element as a secondary resource for further use. It thereby not only makes Cu available again for its designated usage, but also eliminates or at least delays the projected time when a circular steel would be significantly hampered by the accumulated Cu amounts. To address the basic theoretical approach into larger aggregates and charging volumes, technical challenges (e.g., achieving and maintaining the desired atmosphere) and kinetics aspects must be carefully evaluated. For instance, when considering the possibility of implementing the findings of this study in existing EAFs with capacities for treating a several hundred tons,^[45] one should bear in mind the minute portions of the melt (≈1%) that could be actually heated at 2000 °C in the regions that are immediately exposed to the plasma. Therefore, mass transportation toward the reaction front (between the melt and arc) is imperative to be maintained with appropriate convection of the liquid, induced either by magnetic stirring and pulsed arcs for example or enhanced by the geometry of the furnace vessel.^[54] Irrespectively of kinetics aspects for mass transportation, our thermodynamic calculations suggest that substantial evaporation of Cu can also occur at temperatures commonly found in EAF (1650 °C), and not only at the reaction front. Nevertheless, the parallel evaporation of Fe needs to be considered (Figure 8), as well as the role of graphite as the electrode material. The scalability also needs to consider the most suitable refractory linings to preserve inner structures of the arc melting furnaces against the aggressive arc radiation and FeO-containing melts.^[53] This is especially relevant as existing EAFs are currently designed to operate with a small fraction of slags,^[45] i.e., melts with low content of oxygen, differently from the mixtures utilized in our laboratory scale experiments. Similarly important are technological solutions to capture the evaporated Cu. Iron ores are also accompanied of minor fractions of gangue-related intruding tramp elements such as sulfur, phosphorus, and others, elements that might be detrimental to the properties of the produced steel. Therefore, the purification of such elements should also be considered in the process either via their preferential evaporation, by exploiting the fact that most of gangue oxides existing in iron ores have higher vapor pressure

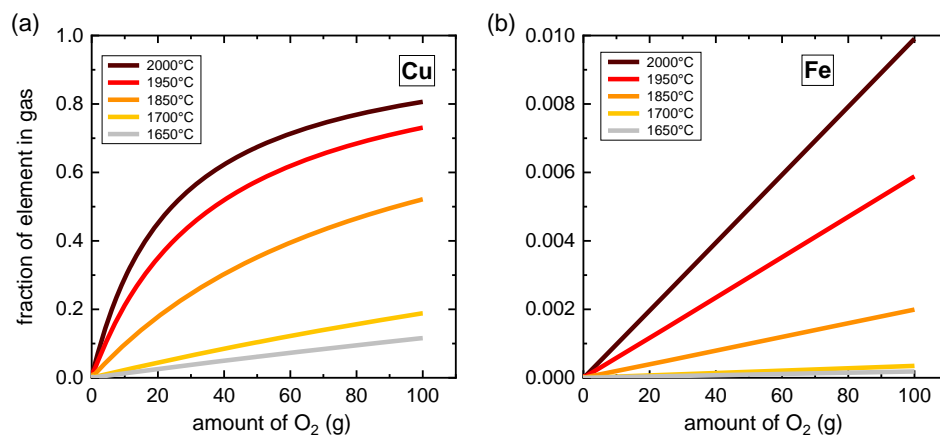


Figure 8. Equilibrium between a Fe–1%Cu–22%O melt and different amounts of oxygen present in air at temperatures varying from 1650 to 2000 °C. a) Fractions of the total Cu partitioned into the gas phase as a function of the provided oxygen at 2000 °C. b) Corresponding fractions of Fe evaporated.

than that of iron and its oxides;^[29] or via the deliberative addition of slag forming compounds to adjust the chemistry of the bath and permit mass partitioning of undesired elements into the slag portion^[55] while simultaneously maintaining the global oxygen content around the critical one to enhance Cu evaporation. Only by addressing these aspects in large scales, a suitable energy balance can be properly evaluated, thus helping the process operate at optimized energy consumption. These observations together with the scientific findings reported here aim at supporting the development of the next generation of green steel reactors currently found in pilot-plant scale.^[56]

5. Conclusion

The increasing Cu contamination in steel scraps, especially coming from electrical components of vehicles, represents a huge challenge to steel recycling and is projected to impede a future circular steel economy. Removing Cu from Fe-based melts is hampered by thermodynamic constraints, and Cu in recycled steel acts detrimental to its integrity during thermomechanical processing (hot shortness). Here, we provide results that offer a new perspective for removing Cu from Fe–Cu–O melts using arc melting furnaces, by using the contaminated scrap-based material in the primary production of iron as long as it is still required on a huge global scale until a circular steel economy is viable. We found that the evaporation of Cu from Fe–Cu–O melts is highly dependent on its O concentration. The maximum removal of Cu via evaporation occurs at the critical O composition of 22 wt%, where the activity of Cu in the molten Fe–Cu–O mixture is maximized. These findings suggest that we can charge Cu-containing steel scraps together with iron ores in a plasma reactor so that the final global O composition lies around the critical one. By melting this mixture with an inert plasma or under an oxidizing atmosphere, the evaporation of Cu is favored and the purified resulting Fe–O melt could be readily used for a subsequent reduction step using hydrogen or circular carbon-based substances as reducing agents. Before the implementation of the proposed method into industrial reactors, technical aspects should be considered, including solutions for collection of Cu from the gas phase, adoption of adequate slag-forming compounds, and suitable refractory linings. Mass transport toward the reaction interface is mandatory to be achieved through liquid convection, either induced by the transferred arcs themselves or enhanced by magnetic stirring. By implementing all of these items, energy balance monitoring can be appropriately employed. With this work, we aim to provide scientific-based evidences to open the possibility of combining recycling, purification, and iron manufacturing in one single reactor for future green and clean steel production, while simultaneously collecting valuable Cu for secondary use—and not simply diluting it in steel products.

Acknowledgements

The authors are greatly thankful to Michael Kulse (MPIE) for the hydrogen plasma reduction experiments, Benjamin Breitbach (MPIE) for the support with the XRD measurements, and Daniel Kurz (MPIE) for the chemical analysis. Dr. Ankita Mahajan is also deeply acknowledged for her kind

assistance along the development of this work. Mr. Tianyi You is highly acknowledged for his assistance with the graphics drawing. I.R.S.F. acknowledges financial support through CAPES and Alexander von Humboldt Foundation (grant no. 88881.512949/2020-01). H.S. acknowledges funding by the Heisenberg Program of the Deutsche Forschungsgemeinschaft (DFG, German Research Foundation), project number: 416498847. The authors also acknowledge funding by the European Union through the ERC Advanced Grant “ROC” (grant agreement no. 101054368). Views and opinions expressed are however those of the author(s) only and do not necessarily reflect those of the European Union the ERC. Neither the European Union nor the granting authority can be held responsible for them.

Open Access funding enabled and organized by Projekt DEAL.

Conflict of Interest

The authors declare no conflict of interest.

Author Contributions

I.R.S.F. and H.S. conceptualized the work and analyzed the experimental data. I.R.S.F. and A.K.S. performed the thermodynamic simulations. I.R.F.S. and Ö.K.B. conducted the microstructural analysis. Ö.K.B. prepared the samples for the corresponding characterization. I.R.S.F., D.R., and H.S. wrote the original manuscript. All the authors discussed in high detail the obtained findings and commented on the written manuscript.

Data Availability Statement

The data that support the findings of this study are available from the corresponding author upon reasonable request.

Keywords

Cu removal, electric arc furnaces, Fe–Cu–O melts, steel recycling, steel scrap, sustainable ironmaking

Received: November 16, 2023

Revised: January 10, 2024

Published online: February 12, 2024

- [1] D. Raabe, C. C. Tasan, E. A. Olivetti, *Nature* **2019**, 575, 64.
- [2] Bureau of International Recycling, World Steel Recycling in Figures 2016–2020, Steel Scrap – a Raw Mater, *Steelmak* **2021**, <https://www.bir.org/publications/facts-figures/download/821/175/36?method=view>.
- [3] C. Graedel, T. E. Allwood, J. Birat, J.-P. Reck, B. K. Sibley, S. F. Sonnemann, G. Buchert, M. Hagelüken, UNEP, Recycling Rates of Metals – A Status Report, A Report of the Working Group on the Global Metal Flows to the International Resource Panel **2011**, <https://mmta.co.uk/wp-content/uploads/2015/01/UNEP-Report-Recycling-rates-of-metals-2011.pdf>.
- [4] S. Pauliuk, R. L. Milford, D. B. Müller, J. M. Allwood, *Environ. Sci. Technol.* **2013**, 47, 3448.
- [5] J. Allwood, *Mater. World.* **2016**, 24, 44.
- [6] B. B. Çiftçi, Maximising Scrap use Helps reduce CO₂ Emissions, World Steel Association n.d. <https://worldsteel.org/steel-topics/raw-materials/> (accessed: July 2022).

- [7] IEA, Global Crude Steel Production by Process Route and Scenario, 2019–2050 **2020**, <https://www.iea.org/data-and-statistics/charts/global-crude-steel-production-by-process-route-and-scenario-2019-2050>.
- [8] K. E. Daehn, A. Cabrera Serrenho, J. M. Allwood, *Environ. Sci. Technol.* **2017**, *51*, 6599.
- [9] K. E. Daehn, A. C. Serrenho, J. Allwood, *Metall. Mater. Trans. B: Process Metall. Mater. Process. Sci.* **2019**, *50*, 1225.
- [10] D. Panasiuk, I. Daigo, T. Hoshino, H. Hayashi, E. Yamasue, D. H. Tran, B. Sprecher, F. Shi, V. Shatokha, *J. Ind. Ecol.* **2022**, *26*, 1040.
- [11] I. Kapoor, C. Davis, Z. Li, *Ironmak. Steelmak.* **2021**, *48*, 712.
- [12] K. Daehn, R. Basuhi, J. Gregory, M. Berlinger, V. Somjit, E. A. Olivetti, *Nat. Rev. Mater.* **2022**, *7*, 275.
- [13] A. de Koning, R. Kleijn, G. Huppel, B. Sprecher, G. van Engelen, A. Tukker, *Resour. Conserv. Recycl.* **2018**, *129*, 202.
- [14] Copper Development Association Inc, Copper in Electric Vehicles, Electr. Veh. n.d., <https://copper.org/environment/sustainable-energy/electric-vehicles/> (accessed July 2022).
- [15] K. Nakajima, O. Takeda, T. Miki, K. Matsubae, T. Nagasaka, *Environ. Sci. Technol.* **2011**, *45*, 4929.
- [16] D. Savov, L. Volkova, E. Janke, *Mater. Geoenvironment.* **2003**, *50*, 627–640.
- [17] L. M. Lombrana, Saving the Planet With Electric Cars Means Strangling This Desert, Bloom. Green Hyperdrive **2019**, <https://www.bloomberg.com/news/features/2019-06-11/saving-the-planet-with-electric-cars-means-strangling-this-desert>.
- [18] A. I. Zaitsev, N. E. Zaitseva, E. K. Shakhpazov, B. M. Mogutnov, *ISIJ Int.* **2004**, *44*, 639.
- [19] T. Yoshida, T. Nagasaka, M. Hino, *ISIJ Int.* **2001**, *41*, 706.
- [20] L. G. Garza, C. J. Van Tyne, *J. Mater. Process. Technol.* **2005**, *159*, 169.
- [21] IEA, Iron and Steel Technology Roadmap - Part of Energy Technology Perspectives **2020**, <https://www.iea.org/reports/iron-and-steel-technology-roadmap>.
- [22] C. Hoffmann, M. Van Hoey, B. Zeumer, *Decarbonization Challenge for Steel Hydrogen as a Solution in Europe*, McKinsey Co. **2020**.
- [23] F. Patisson, O. Mirgautx, *Metals* **2020**, *10*, 1.
- [24] E. Basson, *Yearb. World Steel Assoc.* **2020**, *2020*, 1.
- [25] Y. Ma, I. R. Souza Filho, Y. Bai, J. Schenk, F. Patisson, A. Beck, J. A. van Bokhoven, M. G. Willinger, K. Li, D. Xie, D. Ponge, S. Zaefferer, B. Gault, J. R. Mianroodi, D. Raabe, *Scr. Mater.* **2022**, *213*, 114571.
- [26] D. Spreitzer, J. Schenk, *Steel Res. Int.* **2019**, *90*, 1900108.
- [27] S.-H. Kim, X. Zhang, Y. Ma, I. R. Souza Filho, K. Schweinar, K. Angenendt, D. Vogel, L. T. Stephenson, A. A. El-Zoka, J. R. Mianroodi, M. Rohwerder, B. Gault, D. Raabe, *Acta Mater.* **2021**, *212*, 116933.
- [28] S. Lang, M. Köpf, R. Valery, A. Orth, *Circored Fine Ore Direct Reduction – A Proven Process to Decarbonize Steelmaking*, *Stahl + Eisen* **2022**. <https://www.stahleisen.de/2022/09/12/circored-fine-ore-direct-reduction-a-proven-process-to-decarbonize-steelmaking/>.
- [29] I. R. Souza Filho, Y. Ma, M. Kulse, D. Ponge, B. Gault, H. Springer, D. Raabe, *Acta Mater.* **2021**, *213*, 116971.
- [30] I. R. Souza Filho, H. Springer, Y. Ma, A. Mahajan, C. C. da Silva, M. Kulse, D. Raabe, *J. Clean. Prod.* **2022**, *340*, 130805.
- [31] M. Naseri Seftejani, J. Schenk, *Metals* **2018**, *8*, 1051.
- [32] M. Naseri Seftejani, J. Schenk, D. Spreitzer, M. Andreas Zarl, *Materials* **2020**, *13*, 935.
- [33] M. Naseri Seftejani, J. Schenk, M. A. Zarl, *Materials* **2019**, *12*, 1608.
- [34] H. Hiebler, J. F. Plaul, *Metalurgija* **2004**, *43*, 155.
- [35] J. F. Plaul, W. Krieger, E. Bäck, *Steel Res. Int.* **2005**, *76*, 548.
- [36] T. Matsuo, *Tetsu-To-Hagane/J. Iron Steel Inst. Jpn.* **1989**, *75*, 82.
- [37] T. Matsuo, *Trans. Iron Steel Inst. Jpn.* **1988**, *28*, 319.
- [38] T. Nishi, S. Fukagawa, K. Shinme, T. Matsuo, *ISIJ Int.* **1999**, *39*, 905.
- [39] D. R. Henri Pauna, D. Ernst, M. Zarl, I. R. Souza Filho, H. Springer, M. Huttula, J. Schenk, Timo Fabritius, in *6th Eur. Steel Technol. Appl. Days*, Düsseldorf **2023**.
- [40] B. Hallstedt, D. Risold, L. J. Gauckler, *J. Phase Equilibria.* **1994**, *15*, 483.
- [41] A. V. Khvan, O. B. Fabrichnaya, G. Savinykh, R. Adam, H. J. Seifert, *J. Phase Equilibria Diffus.* **2011**, *32*, 498.
- [42] B. Sundman, *J. Phase Equilibria.* **1991**, *12*, 127.
- [43] M. Selleby, B. Sundman, *Calphad* **1996**, *20*, 381.
- [44] I. R. Souza Filho, Y. Ma, D. Raabe, H. Springer, *JOM* **2023**, *75*, 2274.
- [45] H. J. Odenthal, A. Kemminger, F. Krause, L. Sankowski, N. Uebber, N. Vogl, *Steel Res. Int.* **2018**, *89*, 1700098.
- [46] K. C. Sabat, A. B. Murphy, *Metall. Mater. Trans. B* **2017**, *48*, 1561.
- [47] K. Kamiya, N. Kitahara, I. Morinaka, K. Sakuraya, M. Ozawa, M. Tanaka, *Trans. Iron Steel Inst. Jpn.* **1984**, *24*, 7.
- [48] J. B. Ott, J. Boerio-Goates, *Chemical Thermodynamics: Advanced Applications*, Elsevier, Amsterdam **2000**, pp. 1–42, https://www.google.com/search?sca_esv=6dcea3799f814f53&rlz=1C1GCEU_enIN1078IN1078&q=Amsterdam&si=AKbGX_obynta-BNzZrFs5Xp6xpKKQhp3e6ZAEtk9w76AgBhATfr-0uD9j0WKn96jQoxUYID3IPmvUwLn2W_ZazhiO8YKrrlCUOPRG5MkaKYFwtaoDOHih64hiQ6tsQZ8RObK24Dn_Xplhkaim5c68CU4e1bMbdeHz_3v7HHod1DXvhBnlsaTgnAdrN0BW's0dxBbo7-T11Q&sa=X&ved=2ahUKEwio-bGUypKEAxUAT2wGHY7IBjkQmxMoAXoECEwQAw.
- [49] J. G. Calvert, *Pure Appl. Chem.* **1990**, *62*, 2167.
- [50] S. M. Mike Parr, What is the real cost of green hydrogen? **2020**, <https://www.euractiv.com/section/energy/opinion/what-is-the-real-cost-of-green-hydrogen/> (accessed: July 2021).
- [51] M. Noussan, P. P. Raimondi, R. Scita, M. Hafner, *Sustainability* **2020**, *13*, 298.
- [52] G. Cavaliere, Analysis on Copper, Lead and Tin Removal in Steel Scrap Sorting Technologies Involved, Environmental Considerations and Economic Aspects **2023**.
- [53] M. Ribeiro Gomes, T. Leber, T. Tillmann, D. Kenn, D. Gavagnin, T. Tonnesen, J. Gonzalez-Julian, *J. Eur. Ceram. Soc.* **2023**, *44*, 1307.
- [54] P. Cavaliere, *Clean Ironmaking and Steelmaking Processes*, Springer International Publishing, Cham **2019**, pp. 303–375, https://doi.org/10.1007/978-3-030-21209-4_6.
- [55] O. Kovtun, M. Karbayev, I. Korobeinikov, C. Srishilan, A. K. Shukla, O. Volkova, *Steel Res. Int.* **2021**, *92*, 9.
- [56] M. A. Zarl, D. Ernst, J. Cejka, J. Schenk, *Materials* **2022**, *15*, 4767.
- [57] <https://www.whichcar.com.au/news/bentley-release-amazing-photos-of-its-bentayga-suv-electrical-system>.